metals

MDPI

Article

Annealing Effect in Amorphous Fe-Co-B-Si-Nb According to Fe/Co Ratio

Hyunsol Son [1], Jihye Park [1], Hyunkyung Lee [1] and Haein Choi-Yim [1,2,*]

[1] Department of Applied Physics, Sookmyung Women's University, Seoul 04310, Republic of Korea; 96gustof@sookmyung.ac.kr (H.S.); jihye818@sookmyung.ac.kr (J.P.); 2hyunkyung@sookmyung.ac.kr (H.L.)
[2] Institute of Advanced Materials and Systems, Sookmyung Women's University, Seoul 04310, Republic of Korea
* Correspondence: haein@sookmyung.ac.kr

Abstract: These days, electric motor qualities and energy-saving problems are significant to our society. The critical component of these problems is related to magnetic materials. In this respect, here, we investigated the $(Fe_xCo_{1-x})_{72}B_{19.2}Si_{4.8}Nb_4$ ($0 \leq x \leq 1$, at 0.1 intervals) ribbon alloys' structural, thermal, and magnetic properties. Replacing Co with Fe turned out to increase saturation magnetization up to 127.7 emu/g and improve thermal stability. Additionally, we conducted heat treatment at 843, 893, and 943 K for 10 mins, and the annealing effect in the amorphous $(Fe_xCo_{1-x})_{72}B_{19.2}Si_{4.8}Nb_4$ ($0.4 \leq x \leq 0.9$, at 0.1 intervals) ribbons on structural and magnetic properties are analyzed. The saturated magnetization (M_s) value has increased by about 20 to 30 emu/g by the heat treatment and tends to increase as the annealing temperature increases until the annealing temperature approaches 893 K. After annealing at 943 K for 10 mins, the highest saturation magnetization of 156.8 emu/g was achieved. In addition, all four samples show the same coercivity trend. The coercivity decreases when the initial heat treatment at 843 K is applied to the ribbons. However, after annealing at this high temperature, such as 893, 943 K, the Fe_3B, and $(Fe, Co)_{23}B_6$ phases are also generated and cancel out the good soft magnetic properties of α-(Fe, Co) phase.

Keywords: amorphous; annealing; nanocrystallites; soft magnetic properties; glass forming ability; crystallization temperature

check for updates

Citation: Son, H.; Park, J.; Lee, H.; Choi-Yim, H. Annealing Effect in Amorphous Fe-Co-B-Si-Nb According to Fe/Co Ratio. *Metals* **2023**, *13*, 715. https://doi.org/10.3390/met13040715

Academic Editor: Elena Panchenko

Received: 1 March 2023
Revised: 30 March 2023
Accepted: 4 April 2023
Published: 5 April 2023

Copyright: © 2023 by the authors. Licensee MDPI, Basel, Switzerland. This article is an open access article distributed under the terms and conditions of the Creative Commons Attribution (CC BY) license (https://creativecommons.org/licenses/by/4.0/).

1. Introduction

The development of soft magnetic materials with improved properties has become increasingly important in recent years due to the emergence of energy problems such as the need for low carbon and nature-harmonious societies [1]. In order to reduce electricity consumption and physical dimensions, there is a need for transformers and motors with improved energy efficiency [2,3]. This requires the development of a new material with excellent soft magnetic properties that can withstand severe operating conditions such as high temperature and frequency [4–6]. Moreover, the demand for soft magnetic materials is not limited to energy-related applications, but also includes various other industries such as telecommunications and automotive [7]. As technology advances and new applications emerge, the need for soft magnetic materials with good performance in harsh environments continues to grow. Therefore, researchers and engineers are constantly exploring new materials and manufacturing techniques to meet the increasing demand for high-performance soft magnetic materials. These efforts not only contribute to the advancement of technology, but also play a crucial role in addressing the global energy and environmental challenges we face today.

In this respect, Fe-based and Co-based amorphous alloys have good soft magnetic properties such as high permeability and low core loss due to random magnetic anisotropy and exhibit high strength and corrosion resistance [1,8,9]. In addition, replacing the Co with the Fe improves the saturation magnetization (M_s) according to the Slater-Pauling

curve [10]. Additionally, the addition of Co to the Fe-based amorphous alloy improves the high-temperature magnetic properties of the alloy [11–14], and greatly increases the glass-forming ability (GFA) through melting and liquidus temperature reduction [15]. Accordingly, the (Fe, Co)-B-Si alloy system, in which metalloid elements were added to improve GFA and expand the supercooling region, was developed in 1974 and had excellent soft magnetic properties and high strength compared to other Fe-B-Si systems [16–18]. However, since B and Si reduce the magnetic moment of the material [4,19], adding a small amount of Nb that does not reduce soft magnetic properties to replace metalloids (Si and B) in Fe-Co amorphous alloys can lead to good GFA and thermal stability through its low diffusion coefficient and the formation of network-like atomic configurations [9,15,20,21]. Furthermore, recent studies have shown that Fe-Co-B-Si-Nb alloys also possess other advantageous properties. For example, they exhibit high mechanical strength, good corrosion resistance, and excellent thermal stability [4,10,20,22,23]. These properties make Fe-Co-B-Si-Nb alloys suitable for use in various applications, such as magnetic cores for high-frequency transformers and motors, magnetic shielding materials, and magnetic sensors [24].

Despite such improved mechanical properties, glass-forming ability, and thermal stability, amorphous alloys still have limitations in their soft magnetic properties being significantly degraded under high frequencies due to their metastable state and the absence of magnetic domain walls [4,25–27]. This can be optimized for applications by removing residual stress and reducing magneto-crystalline anisotropy by exchange-coupled with fine ferromagnetic nanocrystallites and surrounded amorphous matrix through heat treatment [4,23,28–32]. For Fe-based amorphous alloys, mainly used in soft magnetic applications, the first crystalline phase precipitated at the lowest temperature is most likely α-Fe, which contributes primarily to high magnetization [2]. Therefore, an appropriate heat treatment temperature is usually within the range between the end of the first crystallization and the beginning of the second crystallization, which effectively controls the volume fraction, precipitate size, and distribution of α-Fe [33].

Typical examples of commercial nanocrystalline alloy systems include FINEMET (Hitachi Metals Ltd., Tokyo, Japan) (Yoshizawa et al., 1988), Nanoperm (MH&W International Corp., Mahwah, New Jersey, USA) (Suzuki et al., 1991a, 1991b), and HITPERM (Carnegie Mellon University, Pittsburgh, PA, USA) (Willard et al., 1998). FINEMET was first developed by Yoshizawa in 1988 and has a specific microstructure characterized by randomly oriented submicron-sized α-FeSi particles and a bcc structure, which has high initial permeability and low saturation magnetostriction but has lower magnetic saturation flux density compared to Si steel [2,34–36]. Additionally, Nanoperm exhibits high magnetic saturation flux density values of 1.5–1.7 T but includes expensive and easily oxidizable elements such as Zr and Hf [2]. HITPERM has a high Curie temperature but has a maximum coercivity of 200 A/m and high material costs due to the addition of a large amount of Co [2,37].

Although Fe-based alloys exhibit excellent soft magnetic properties at ambient temperatures, their limited thermal stability and Curie temperatures below 700 K lead to a loss of magnetic ordering at high temperatures, making them unsuitable for high-temperature applications [7,38,39]. To overcome these limitations, recent reports suggest incorporating cobalt into nanocrystalline systems to achieve superior soft magnetic properties coupled with high-temperature magnetic stability [7,24,40].

In our study, an amorphous alloy has been developed based on Co-B-Si-Nb, where Co has been partially substituted by Fe. We aim to explore the effect of Fe/Co ratio variation in the (Fe, Co)$_{72}$B$_{19.2}$Si$_{4.8}$Nb$_4$ alloy system from 0 to 1.0 at 0.1 intervals on its thermal and magnetic properties. In addition, we investigate the changes in the structural and magnetic properties of the (Fe$_x$Co$_{1-x}$)$_{72}$B$_{19.2}$Si$_{4.8}$Nb$_4$ alloy system in response to the thermal treatment. Specifically, we examine the impact of varying Fe/Co ratios ranging from 0.4 to 0.9 at 0.1 intervals of the (Fe$_x$Co$_{1-x}$)$_{72}$B$_{19.2}$Si$_{4.8}$Nb$_4$ alloy system on the microstructural and magnetic property changes according to different annealing temperatures. To achieve the best microstructure, saturation magnetization, and coercivity, the amorphous ribbon pre-

cursors created through melt spinning undergo annealing at several specific temperatures higher than the primary crystallization temperature (T_x).

Our study is expected to contribute to the development of novel magnetic materials with superior properties for high-temperature applications. By exploring the impact of Fe/Co ratio variation on the thermal and magnetic properties of the $(Fe_xCo_{1-x})_{72}B_{19.2}Si_{4.8}Nb_4$ alloy system, we can gain insights into the mechanisms underlying the observed changes and optimize the alloy composition and annealing temperature to achieve desired properties.

2. Materials and Methods

Alloy ingots with the nominal atomic percentage composition of $(Fe_xCo_{1-x})_{72}B_{19.2}Si_{4.8}Nb_4$ ($0 \leq x \leq 1$, at 0.1 intervals) were prepared with an arc-melting technique under a Ti-gettered high-purity argon atmosphere. Raw materials with high purity of Fe (99.95%), Co (99.95%), B (99.5%), Si (99.999%), and Nb (99.95%) were melted four times for homogeneous mixing of the alloys. After the ingot manufacturing process, amorphous ribbons were fabricated by casting molten ingots onto a fast-rolling single copper wheel speed of 51 m/s. All melt-spinning processes were performed at a vacuum level of 10^{-5} torr in a chamber equipped with a diffusion pump. The loading amount of the sample was 6 g at a time, and the average width and thickness of the fabricated ribbons were 2–3 mm and 0.02–0.03 mm, respectively. The detailed atomic distribution of the as-spun ribbon was inspected using field emission scanning electron microscope-energy dispersive x-ray spectroscopy (SEM-EDS). To confirm the rapid solidification status and phase analysis, x-ray diffraction (XRD, D8 Advance, Bruker, Billerica, MA, USA) was used at an accelerating voltage of 40 kV, current of 40 mA, scanning rate of 2.4°/min, and two theta ranges of 20° to 80°, and Cu-Kα was used as the target. In addition, the magnetic characteristics of the rapidly solidified amorphous ribbon were examined using a vibrating sample magnetometer (VSM, EV9, MicroSense, Lowell, MA, USA) to investigate the magnetization behaviors when applying the maximum applied field of 10,000 Oe. Differential scanning calorimetry (DSC, Labsys N-650, SINCO, Seoul, Korea) was measured on amorphous ribbons to determine the appropriate heat treatment temperature and assess glass-forming ability (GFA) under argon flow and heating rate of 0.34 °C/s, and maximum heating temperature of 1200 °C. Based on the DSC outcome, nanocrystallization in the amorphous matrix was conducted by isothermal annealing under vacuum at different temperatures for 10 mins, followed by water quenching. The crystallized structure was determined by x-ray diffraction with Cu-Kα radiation. Phase identification was concluded through the software Bruker DIFFRAC.EVA v4.3.1. Comparison of amorphous and annealed samples' magnetic properties, such as saturation magnetization (M_s), proceeded with a vibrating sample magnetometer under an in-plane applied magnetic field ranging from −10,000 to 10,000 Oe.

3. Results and Discussion

All specimens were measured by scanning electron microscopy–energy dispersive X-ray spectroscopy (SEM-EDS) to confirm that all elements are evenly mixed. Figure 1 shows the SEM-EDS spectrum for each element for the $(Fe_xCo_{1-x})_{72}B_{19.2}Si_{4.8}Nb_4$ (x = 0.7) as-spun ribbon. Consequently, it is clearly shown that the as-spun ribbon is chemically homogeneously mixed.

Figure 2 shows x-ray diffraction (XRD) patterns of the $(Fe_xCo_{1-x})_{72}B_{19.2}Si_{4.8}Nb_4$ ($0 \leq x \leq 1$, at 0.1 intervals) as-spun ribbons. Since the patterns show broad halo humps around $2\theta = 45°$ without any sharp diffraction peaks, all samples can be assumed to be amorphous. It is clear that all of the alloys have good glass-forming ability (GFA). According to the previous reports, this high GFA appears to be a result of satisfying the following three empirical component rules [10,22,41–44]; (1) multi-component alloy systems composed of three or more elements, (2) significantly different atomic size ratios of about 12% or more between the major three constituent elements, and (3) negative heats of mixing among their elements. Although the atomic size of Co is almost the same as that of Fe, they have significant atomic size mismatches with the other constituent elements, as the radii

are 0.146 nm for Nb atoms, 0.125 nm for Co atoms, 0.111 nm for Si atoms, and 0.09 nm for B atoms [22,44]. These differences in atomic size let the Fe-Co-B-Si-Nb alloy system have a dense packing density. The enthalpy of mixing is −9 kJ/mol for the Co–B pair, −11 kJ/mol for Fe–B pair, −16 kJ/mol for Fe–Nb pair, −18 kJ/mol for Fe–Si pair, −21 kJ/mol for the Co–Si pair, −25 kJ/mol for the Co–Nb pair, and −39 kJ/mol for B–Nb pair [44,45]. Since a large negative mixing enthalpy between each element, it can constitute a thermally stable structure which is beneficial to the glass-forming ability.

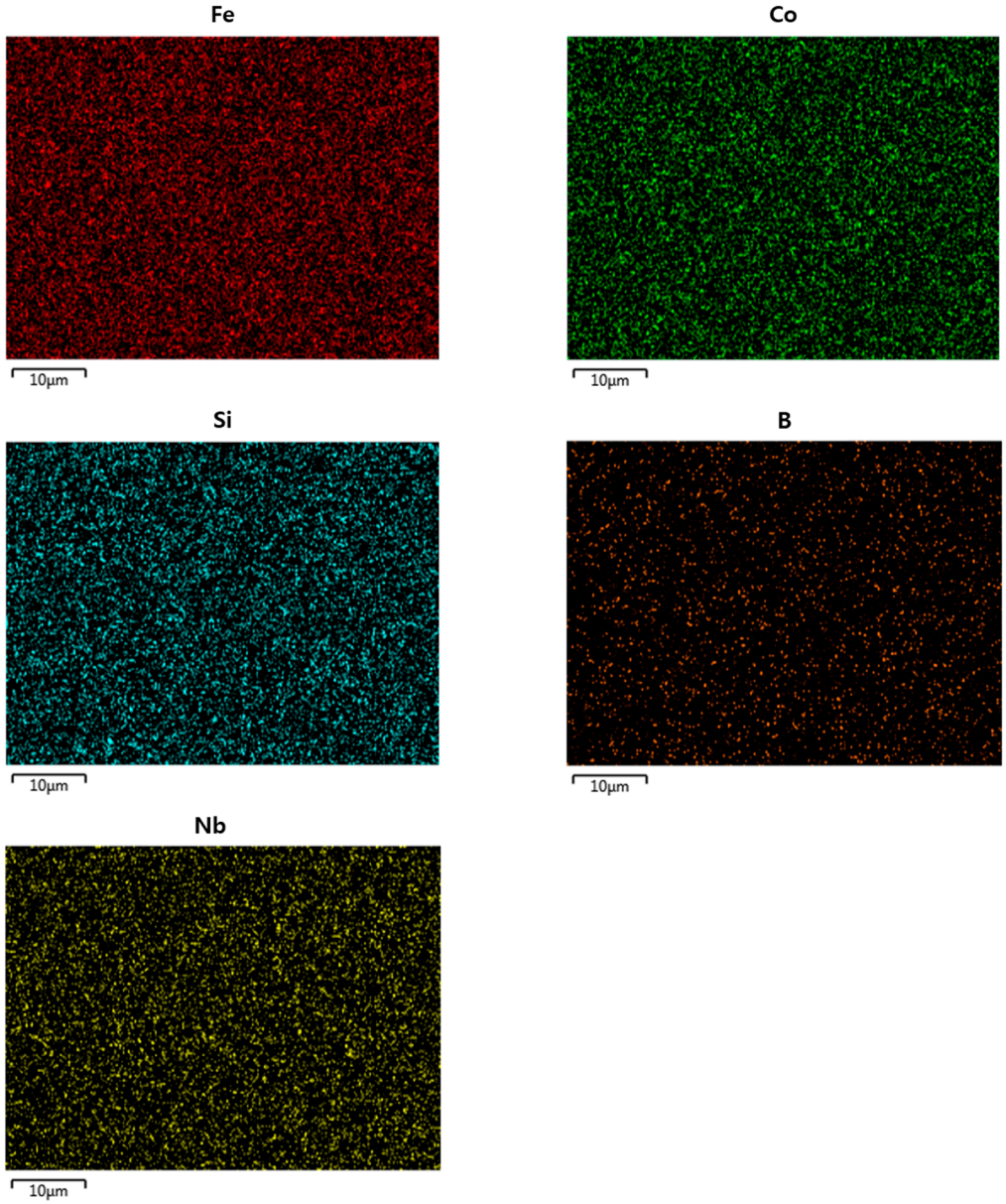


Figure 1. SEM-EDS spectrum for Fe, Co, B, Si, and Nb elements for the as-spun $(Fe_xCo_{1-x})_{72}B_{19.2}Si_{4.8}Nb_4$ (x = 0.7) ribbon.

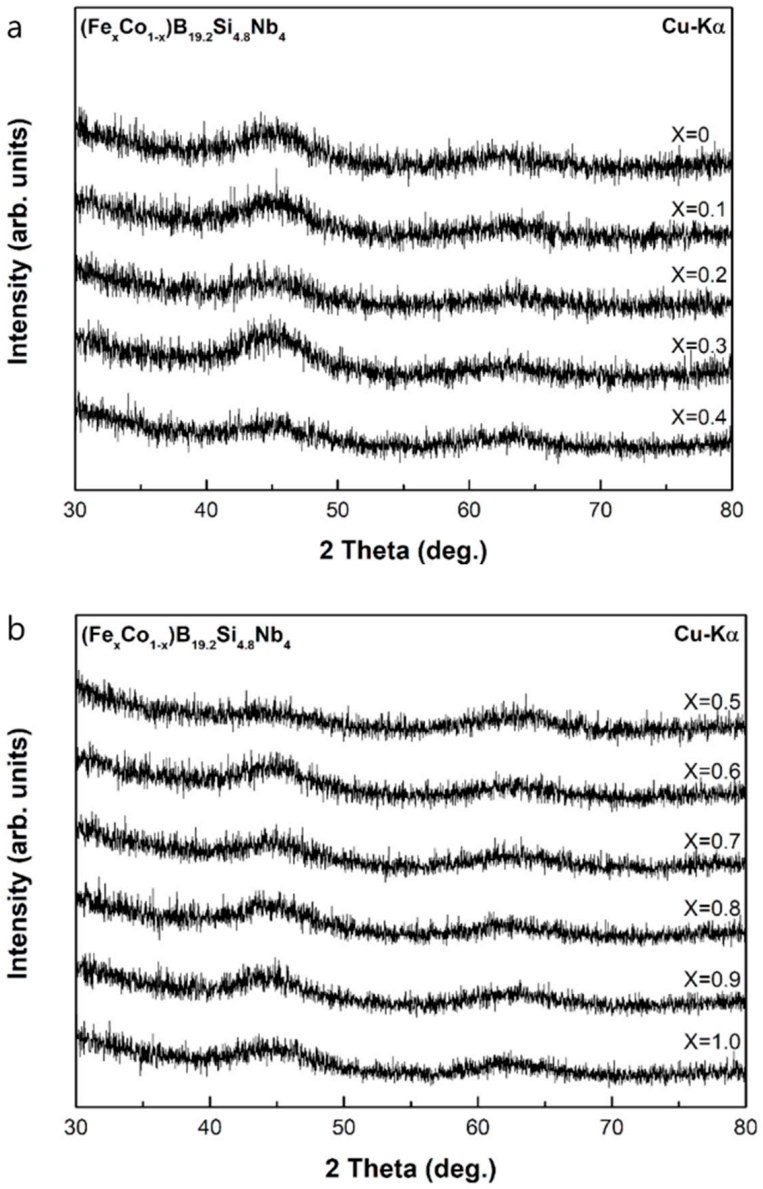


Figure 2. XRD patterns of the $(Fe_xCo_{1-x})_{72}B_{19.2}Si_{4.8}Nb_4$ as-spun ribbons (**a**) $0 \leq x \leq 0.4$ (**b**) $0.5 \leq x \leq 1$.

Figure 3 depicts M-H curves of the $(Fe_xCo_{1-x})_{72}B_{19.2}Si_{4.8}Nb_4$ ($0 \leq x \leq 1$, at 0.1 intervals) as-spun ribbons. All samples seem to have completely square-shaped, and this indicates that all samples are soft magnetic materials with very small coercivity (H_c) values. Each of the saturation magnetization (M_s) values are shown in Table 1, and the tendency of these values according to the Fe content is shown in Figure 4. The M_s value increases almost linearly with increasing Fe substitution to Co through this. Our results exhibit similar tendencies to other previous studies on the magnetic properties of multi-component alloys [23,46–48]. This trend does not follow the Slater-Pauling curve mentioned earlier in the Section 1, which seems to be because the Slater-Pauling curve applies better to the 3D-transition metal alloys [49–51]. Therefore, predicting the saturation magnetization of Fe/Co multi-component alloys as a function of their Fe/Co ratio requires considering the specific characteristics of each alloy, such as the electron count and exchange interaction, magnetic interaction, electron-electron interaction, and structure of each metal because of their complex interactions. In addition, the highest M_s value is 127.7 emu/g for the Fe-only-based alloy $Fe_{72}B_{19.2}Si_{4.8}Nb_4$ ($x = 1$). It seems to be because Fe has a higher magnetic moment than Co [48].

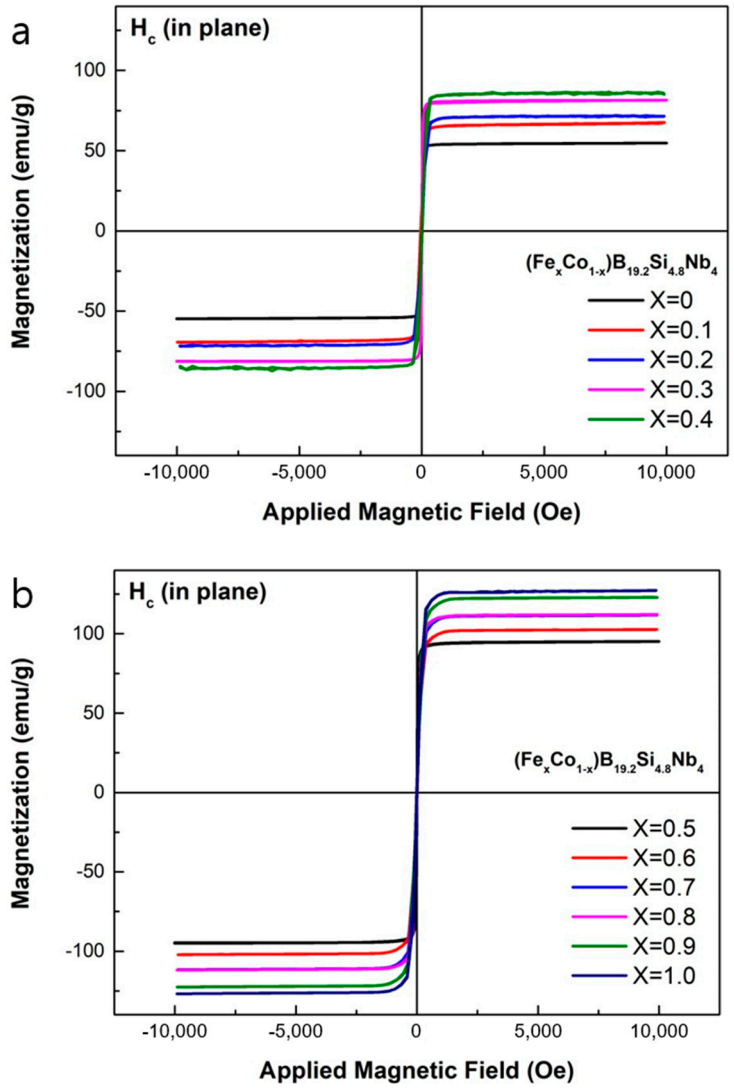


Figure 3. Hysteresis loops of the $(Fe_xCo_{1-x})_{72}B_{19.2}Si_{4.8}Nb_4$ as-spun ribbons (**a**) $0 \leq x \leq 0.4$ (**b**) $0.5 \leq x \leq 1$.

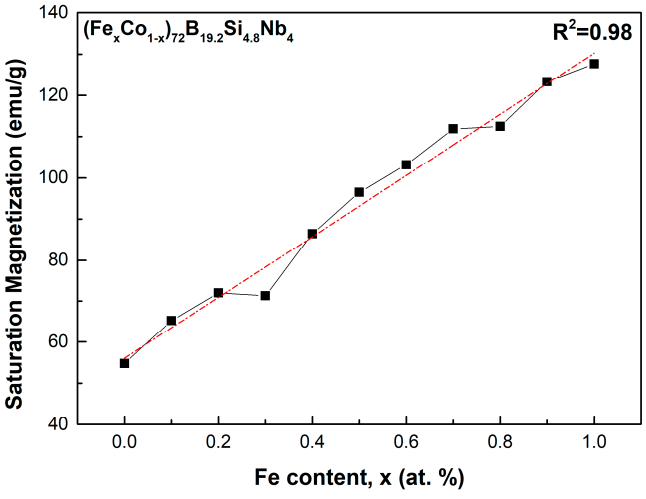


Figure 4. Saturation magnetization tendency of the $(Fe_xCo_{1-x})_{72}B_{19.2}Si_{4.8}Nb_4$ ($0 \leq x \leq 1$, at 0.1 intervals) as-spun ribbons with linear regression analysis corresponding to R^2 value.

Table 1. Thermal and magnetic properties of the $(Fe_xCo_{1-x})_{72}B_{19.2}Si_{4.8}Nb_4$ ($0 \leq x \leq 1$, at 0.1 intervals) as-spun and annealed ribbons.

Alloys $(Fe_xCo_{1-x})_{72}B_{19.2}Si_{4.8}Nb_4$	Annealing Condition [K]	Thermal Properties T_x, [K]	T_g, [K]	Magnetic Property M_s [emu/g]
$Co_{72}B_{19.2}Si_{4.8}Nb_4$ (x = 0)	As-spun	821.2	795.6	54.8
$Co_{64.8}Fe_{7.2}B_{19.2}Si_{4.8}Nb_4$ (x = 0.1)	As-spun	825.8	795.6	65.2
$Co_{57.6}Fe_{14.4}B_{19.2}Si_{4.8}Nb_4$ (x = 0.2)	As-spun	833.8	797.4	72.0
$Co_{50.4}Fe_{21.6}B_{19.2}Si_{4.8}Nb_4$ (x = 0.3)	As-spun	841.5	806.1	71.3
$Co_{43.2}Fe_{28.8}B_{19.2}Si_{4.8}Nb_4$ (x = 0.4)	As-spun	845.8	812.4	86.5
	843			110.2
	893			107.5
	943			108.4
$Co_{36}Fe_{36}B_{19.2}Si_{4.8}Nb_4$ (x = 0.5)	As-spun	850.7	826.1	96.5
	843			112.5
	893			112.6
	943			105.6
$Co_{28.8}Fe_{43.2}B_{19.2}Si_{4.8}Nb_4$ (x = 0.6)	As-spun	848.8	801.6	103.2
	843			129.5
	893			129.6
	943			130.3
$Co_{21.6}Fe_{50.4}B_{19.2}Si_{4.8}Nb_4$ (x = 0.7)	As-spun	851.8	816.3	111.9
	843			138.5
	893			141.1
	943			141.7
$Co_{14.4}Fe_{57.6}B_{19.2}Si_{4.8}Nb_4$ (x = 0.8)	As-spun	853.5	809.1	112.5
	843			144.3
	893			146.2
	943			149.5
$Co_{7.2}Fe_{64.8}B_{19.2}Si_{4.8}Nb_4$ (x = 0.9)	As-spun	856.7	812.0	123.3
	843			146.8
	893			156.1
	943			156.8
$Fe_{72}B_{19.2}Si_{4.8}Nb_4$ (x = 1)	As-spun	853.8	827.1	127.7

The differential scanning calorimetry (DSC) curves measured to analyze the thermal characteristics and set the heat treatment temperature of the amorphous ribbons are shown in Figure 5. According to Figure 5, the glass transition temperature (T_g) and first crystallization temperature (T_x) of $(Fe_xCo_{1-x})_{72}B_{19.2}Si_{4.8}Nb_4$ ($0 \leq x \leq 1$, at 0.1 intervals) tend to increase from 795.6 to 827.1 K and 821 to 856.7 K, respectively as the Fe content increases. A higher T_x is indicative of better thermal stability since structural change occurs at that point. Thus, it is considered that thermal stability and glass-forming ability (GFA) increase with an increase in Fe content. In particular, the increase in GFA is considered to be a phenomenon caused by strengthening the s-d hybrid bonding nature by providing more empty d shells by adding Fe transition elements [46]. A two-stage crystallization process was observed in some compositions, which is related to the crystallization sequence of amorphous alloys. This is probably due to further crystallization of the remaining amorphous or metastable phases, such as bcc-Fe [52]. Accordingly, the heat treatment was conducted for 10 mins for the alloys $(Fe_xCo_{1-x})_{72}B_{19.2}Si_{4.8}Nb_4$ ($0.4 \leq x \leq 0.9$, at 0.1 intervals) to examine the changes in structural and magnetic properties depending on the temperature and the annealing temperature was raised by 50 K starting at 843 K, which is the temperature between the glass transition temperature (T_g) and the first crystallization temperature (T_x). Regarding the annealing time, it was determined, based on the results of several studies, that the average grain/precipitate size decreased when this annealing time was short, while other phases were formed when it was longer than 120 mins [2,4,9,31,46,53–55].

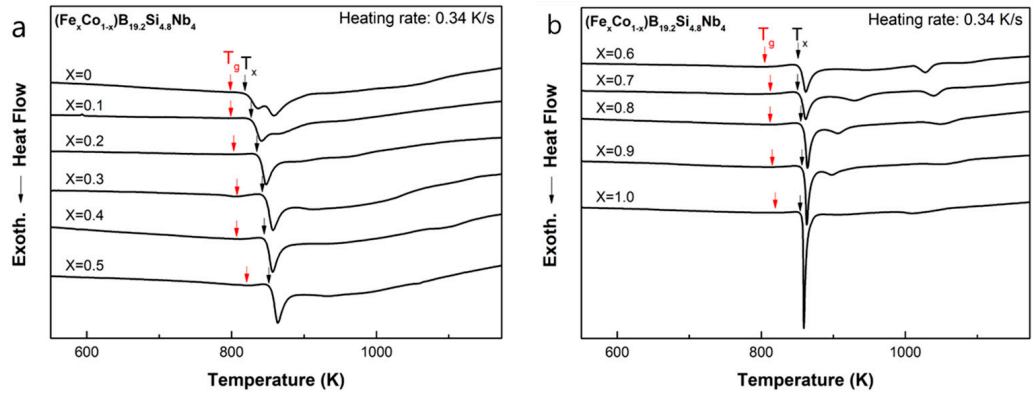


Figure 5. DSC curves of the $(Fe_xCo_{1-x})_{72}B_{19.2}Si_{4.8}Nb_4$ as-spun ribbons (**a**) $0 \leq x \leq 0.5$ (**b**) $0.6 \leq x \leq 1$.

Figure 6 shows the x-ray diffraction (XRD) patterns of the annealed $(Fe_xCo_{1-x})_{72}B_{19.2}Si_{4.8}Nb_4$ ($0.4 \leq x \leq 0.9$, at 0.1 intervals) ribbons for 10 mins. After annealing at 843 K, all of the samples show α-(Fe, Co) phase. However, after annealing over 893 K, Fe_3B, and $(Fe, Co)_{23}B_6$ phase is also created together with the α-(Fe, Co) phase. In particular, it was found that the intensity or the number of peaks corresponding to the Fe_3B phase increases when $x = 0.7$ or higher is annealed, indicating a correlation between the Fe content and the formation of the Fe_3B phase. Thus, it is concluded that the higher the Fe content, the lower the temperature at which the Fe_3B phase is formed. In addition, three phases of α-(Fe, Co), Fe_3B, and $(Fe, Co)_{23}B_6$ precipitated simultaneously upon annealing means that the network-like structure becomes stronger as Fe content increases [27,28]. It also has been reported that the primary precipitation metastable phase of $(Fe, Co)_{23}B_6$ leads to high stability against the crystallization of supercooled liquid [56,57]. Also, when the annealing temperature increases, the intensity tends to be increased because it is normal that the crystalline phase fraction increases in accordance with the annealing temperature [9].

Referring to Figure 7 and Table 1, the saturated magnetization (M_s) value has increased by about 20 to 30 emu/g by the heat treatment, and generally, the saturation magnetization tends to increase as the annealing temperature increases. For example, in the case of $(Fe_xCo_{1-x})_{72}B_{19.2}Si_{4.8}Nb_4$ ($x = 0.8$), the saturation magnetization is gradually increased from 112.5 emu/g to 149.5 emu/g in accordance with annealing temperature. However, in most compositions, when annealing at 893 K or higher, there was no significant M_s improvement effect as in the case of annealing at 843 K for the first time. For instance, in the case of $(Fe_xCo_{1-x})_{72}B_{19.2}Si_{4.8}Nb_4$ ($x = 0.7$), the first heat treatment at 843 K increased 26.6 emu/g compared to the M_s value for as-spun, but when annealed at 893 K, it increased by 2.6 emu/g compared to the 843 K annealed ribbon and when annealed at 943 K, the increase was only 0.6 emu/g. Even when the Fe content is small ($x \leq 0.5$), it was observed that the saturation magnetization decreased. This phenomenon is caused by a higher crystallization amount on Fe_3B and $(Fe, Co)_{23}B_6$ and a lower residual amorphous matrix [4]. In other words, when annealed at 843 K, there were mainly α-(Fe, Co) phases with more ferromagnetic atoms per mole than Fe_3B and $(Fe, Co)_{23}B_6$ phases which greatly increased the saturated magnetization value, but the higher the annealing temperature, the more Fe_3B and $(Fe, Co)_{23}B_6$ phase precipitates, offsetting the overall magnetic moment [4,58]. Nevertheless, it is recommended to conduct the thermal treatment near the first crystallization temperature since it is true that annealing has improved the soft magnetic properties of $(Fe_xCo_{1-x})_{72}B_{19.2}Si_{4.8}Nb_4$ ($0 \leq x \leq 1$, at 0.1 intervals) alloy system.

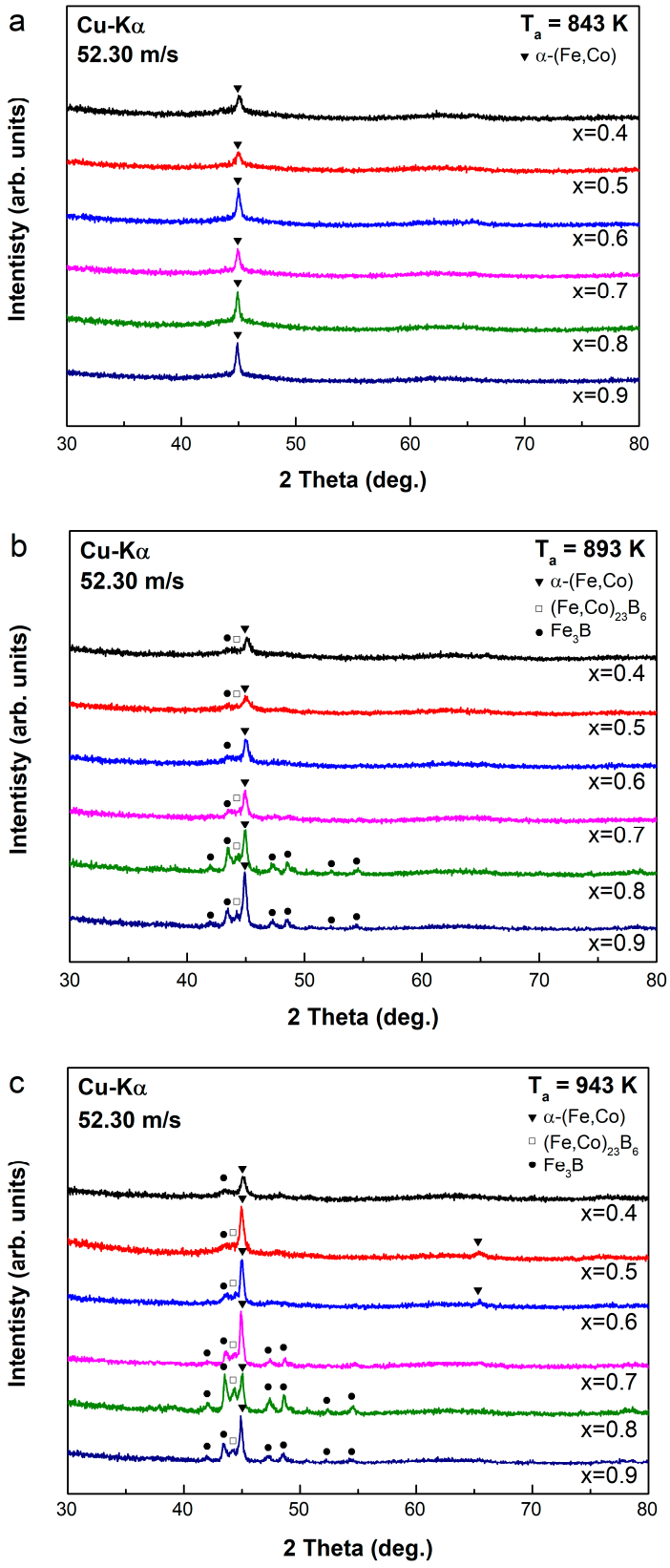


Figure 6. XRD patterns of the annealed $(Fe_xCo_{1-x})_{72}B_{19.2}Si_{4.8}Nb_4$ ($0.4 \leq x \leq 0.9$, at 0.1 intervals) ribbons for 10 mins at (**a**) 843 K (**b**) 893 K (**c**) 943 K.

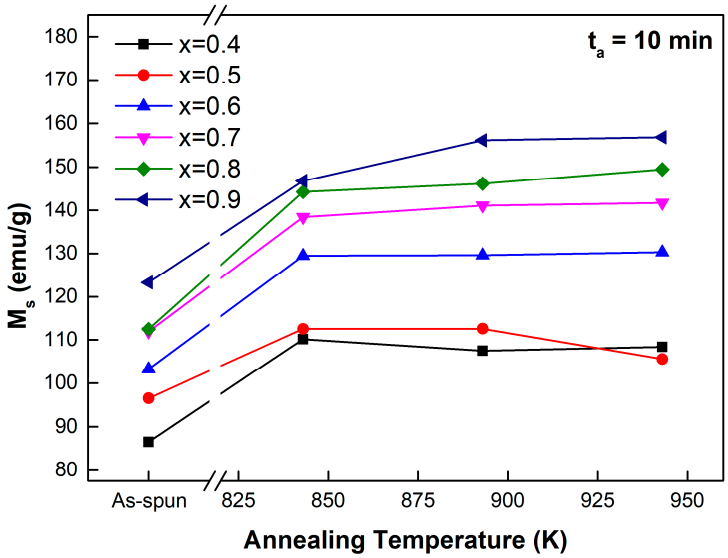


Figure 7. Variation of the saturation magnetization of the $(Fe_xCo_{1-x})_{72}B_{19.2}Si_{4.8}Nb_4$ ($0.4 \leq x \leq 0.9$, at 0.1 intervals) as-spun and annealed ribbons for 10 min at 843, 893, 943 K, respectively.

Figure 8 exhibits the evolution of coercivity (H_c) as a function of the annealing temperature at 843, 893, 943 K for $(Fe_xCo_{1-x})_{72}B_{19.2}Si_{4.8}Nb_4$ ($0.5 \leq x \leq 0.8$, at 0.1 intervals) as-spun and annealed ribbons. The graph was plotted as ln(H_c) values to show the trend better. The coercivity of each alloy showed the same trend; when the initial heat treatment at 843 K was applied to the ribbons, the coercivity decreased, but as the heat treatment progressed to 893 K and 943 K, the coercivity increased. This phenomenon seems to be because coercivity is a structurally sensitive parameter. During the heat treatment process at 843 K, magnetic softening seems to be observed as structural relaxation due to the relaxation of internal stress within the amorphous state [7,47,52,59,60]. In addition, due to insufficient diffusion of atoms, the homogeneous distribution of fine α-(Fe, Co) grains in the amorphous matrix with random magnetic anisotropy cannot be excluded as the cause of the reduction of the coercivity [47,60–63]. In the subsequent heat treatment processes (annealing at 893 and 943 K, respectively), the α-(Fe, Co) grain size increases, acting as a grain coarsening and a pinning center for wall displacement, which seems to have resulted in a magnetic hardening effect [52,55,59,60,63,64]. Furthermore, the formation of strong anisotropic phases, such as Fe_3B (tetragonal structure), and $(Fe, Co)_{23}B_6$ (face-centered cubic structure), results in increased pinning center of magnetic domain wall movement, increasing the coercivity [2,7,53,59].

This study investigates the influence of the Fe/Co ratio on the structural, thermal, and magnetic properties of the Fe-Co-B-Si-Nb system. The results indicate that the alloy design strategy, which involves ferromagnetic elements such as Fe and Co, other glass-forming elements like B and Si, and early transition metals element Nb, is effective in improving the structural integrity of the material. Higher Fe content substantially enhances the glass-forming ability (GFA) and thermal stability of the alloys by increasing their glass transition temperature (T_g) and crystallization temperature (T_x). As the Fe/Co ratio is varied from 100 at. % cobalt to 100 at. % iron, the as-spun amorphous ribbon samples exhibit a significant improvement in saturation magnetization. Optimal annealing treatments lead to lower coercivity and higher saturation magnetization, resulting in improved soft magnetic properties in the nanocrystalline alloy.

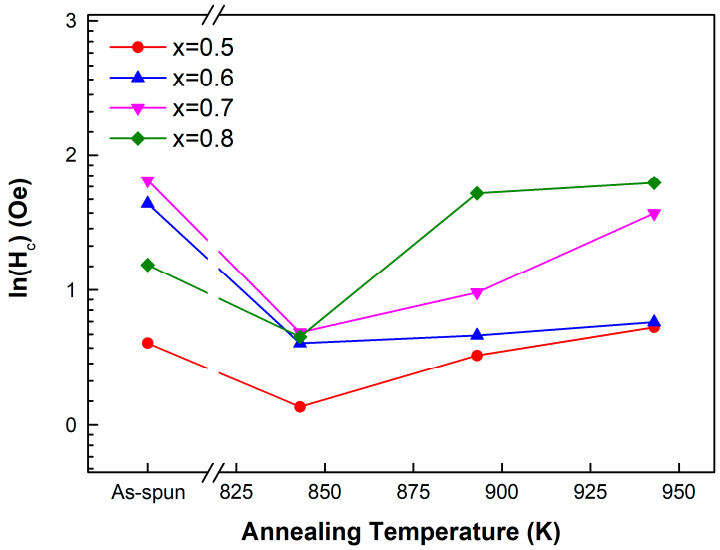


Figure 8. The trend of the coercivity of the $(Fe_xCo_{1-x})_{72}B_{19.2}Si_{4.8}Nb_4$ ($0.5 \leq x \leq 0.8$, at 0.1 intervals) as-spun and annealed ribbons for 10 min at 843, 893, 943 K, respectively.

4. Conclusions

In this study, we observed the effect of changes in the Fe/Co ratio in the $(Fe_xCo_{1-x})_{72}B_{19.2}Si_{4.8}Nb_4$ ($0 \leq x \leq 1$, at 0.1 intervals) alloys on saturation magnetization (M_s) and the crystallization temperature (T_x) and observed the effect of thermal treatment on structural and magnetic properties. The structural characteristics of alloys were measured by X-ray diffraction (XRD) and confirmed that as-spun ribbons were chemically mixed uniformly using scanning electron microscopy-energy dispersive X-ray spectroscopy (SEM-EDS). Magnetic and thermal properties were measured by vibrating sample magnetometer (VSM) and differential scanning calorimetry (DSC). The following conclusions could be drawn.

1. The effects of Fe/Co ratio variation on glass-forming ability (GFA), saturation magnetization (M_s), and crystallization temperature (T_x) are as follows. To prove the certainty of as-spun ribbon fabrication, field emission scanning electron microscopy-energy dispersive X-ray spectroscopy (SEM-EDS) was used to confirm the uniformity of the detailed atomic distribution of the as-spun ribbon. We identified that each element of the scan ribbon $(Fe_xCo_{1-x})_{72}B_{19.2}Si_{4.8}Nb_4$ (x = 0.7) is chemically uniformly mixed. All as-spun samples are completely amorphous, and the saturation magnetization (M_s) values tend to increase with increasing Fe substitution for Co. $Fe_{72}B_{19.2}Si_{4.8}Nb_4$ (x = 1) has the highest saturation magnetization (M_s) value of 127.7 emu/g. In addition, the crystallization temperature (T_x) and glass transition temperature (T_g) tend to increase to 856.7 K and 827.1 K as the Fe content increases. Therefore, replacing Co with Fe improves magnetic and thermal properties.
2. The effect of heat treatment on $(Fe_xCo_{1-x})_{72}B_{19.2}Si_{4.8}Nb_4$ ($0.4 \leq x \leq 0.9$, at 0.1 intervals) as-spun sample characteristics is as follows. We conducted heat treatment at 843 K, 893 K, and 943 K for 10 mins and investigated structural and magnetic property changes. Compared to as-spun ribbons, coercivity (H_c) showed reduced coercivity (H_c) when treated with 843 K in the heat treatment but increased coercivity (H_c) as heat treatment progressed to 893 K and 943 K. The saturation magnetization (M_s) value increased by heat treatment by up to 37 emu/g, but there was no significant saturation magnetization (M_s) improvement annealed at a high temperature compared to annealed at 843 K. After annealing at 843 K, all samples exhibit an α-(Fe, Co) phase, but after annealing above 893 K, the Fe_3B and $(Fe, Co)_{23}B_6$ phases are also produced, deteriorating the soft magnetic properties. In particular, it was confirmed that the intensity or peak number corresponding to more Fe_3B phases increased due to the correlation between the Fe content and the formation of the Fe_3B phase when annealing

was performed at x = 0.7 or more. Therefore, annealing the $(Fe_xCo_{1-x})_{72}B_{19.2}Si_{4.8}Nb_4$ ($0.4 \leq x \leq 0.9$, at 0.1 intervals) alloy system near the first crystallization temperature can improve the soft magnetic properties.

In conclusion, the effect of adding Fe substitution of Co and annealing temperature on structural, thermal, and magnetic properties of $(Fe_xCo_{1-x})_{72}B_{19.2}Si_{4.8}Nb_4$ ($0 \leq x \leq 1$, at 0.1 intervals) alloy was confirmed in this report. Soft magnetic materials are used in electronic devices such as transformers that convert primary electrical energy to magnetic energy and convert secondary electrical energy to magnetic energy, electromagnets that convert electrical energy to rotating power, and generators that generate electricity by electromagnetic induction. This new nanocrystalline alloy material with excellent soft magnetic properties is expected to be widely used in various electromagnetic conversion parts.

Author Contributions: Conceptualization, H.C.-Y.; methodology, H.S., J.P. and H.L.; validation, H.C.-Y., H.S., J.P. and H.L.; formal analysis, H.S. and J.P.; investigation, H.S., J.P. and H.L.; resources, H.C.-Y., H.S., J.P. and H.L.; data curation, H.S., J.P. and H.L.; writing—original draft preparation, H.S., J.P. and H.L.; writing—review and editing, H.S., J.P. and H.L.; visualization, H.S. and J.P.; supervision, H.C.-Y.; project administration, H.C.-Y.; funding acquisition, H.C.-Y. All authors have read and agreed to the published version of the manuscript.

Funding: This work was supported by the Technology Innovation Program (Material Parts Technology Development-Material Parts Package-Type Technology Development Project, 20011368, Development of Thin Film Technology on Soft Magnetic Steel Sheet and Application Technology on Hybrid Permanent Magnet for High Performance Traction Motor) funded by the Ministry of Trade, Industry & Energy (MOTIE, Korea) and also supported by the National Research Foundation of Korea (NRF) grant funded by the Korea government (MSIT) (No.2021R1A2C2008220), equally.

Data Availability Statement: No new data were created or analyzed in this study. Data sharing is not applicable to this article.

Conflicts of Interest: The authors declare no conflict of interest.

References

1. Inoue, A.; Kong, F.L.; Man, Q.K.; Shen, B.L.; Li, R.W.; Al-Marzouki, F. Development and Applications of Fe-and Co-Based Bulk Glassy Alloys and Their Prospects. *J. Alloy. Compd.* **2014**, *615*, S2–S8. [CrossRef]
2. Kwon, S.; Kim, S.; Yim, H.; Kang, K.H.; Yoon, C.S. High Saturation Magnetic Flux Density of Novel Nanocrystalline Core Annealed under Magnetic Field. *J. Alloy. Compd.* **2020**, *826*, 154136. [CrossRef]
3. Kubota, T.; Makino, A.; Inoue, A. Low Core Loss of $Fe_{85}Si_2B_8P_4Cu1$ Nanocrystalline Alloys with High Bs and B800. *J. Alloy. Compd.* **2011**, *509*, S416–S419. [CrossRef]
4. Jia, P.; Wang, E.; Han, K. The Effects of a High Magnetic Field on the Annealing of $[(Fe_{0.5}Co_{0.5})_{0.75}B_{0.2}Si_{0.05}]_{96}Nb_4$ Bulk Metallic Glass. *Materials* **2016**, *9*, 899. [CrossRef]
5. Willard, M.A.; Daniil, M.; Kniping, K.E. Nanocrystalline Soft Magnetic Materials at High Temperatures: A Perspective. *Scr. Mater.* **2012**, *67*, 554–559. [CrossRef]
6. Gutfleisch, O.; Willard, M.A.; Brück, E.; Chen, C.H.; Sankar, S.G.; Liu, J.P. Magnetic Materials and Devices for the 21st Century: Stronger, Lighter, and More Energy Efficient. *Adv. Mater.* **2011**, *23*, 821–842. [CrossRef]
7. Panda, A.K.; Mohanta, O.; Mitra, A.; Jiles, D.C.; Lo, C.C.H.; Melikhov, Y. Soft Magnetic Properties of a High Temperature CoFeSiBNb Nanocrystalline Alloy. *J. Magn Magn Mater.* **2007**, *316*, e886–e889. [CrossRef]
8. O'Handley, R.C. Magnetostriction of Ferromagnetic Metallic Glasses. *Solid State Commun.* **1977**, *21*, 1119–1122. [CrossRef]
9. Abrosimova, G.; Volkov, N.; Orlova, N.; Aronin, A. BCC Nanocrystal Formation in an Amorphous Co-Si-B-Fe-Nb Alloy on Heating. *Mater. Lett.* **2018**, *219*, 97–99. [CrossRef]
10. Shen, B.; Inoue, A.; Chang, C. Superhigh Strength and Good Soft-Magnetic Properties of (Fe, Co)–B–Si–Nb Bulk Glassy Alloys with High Glass-Forming Ability. *Appl. Phys. Lett.* **2004**, *85*, 4911–4913. [CrossRef]
11. Wang, J.; Wang, Z.; Jia, Y.; Shi, R.; Wen, Z. High Temperature Soft Magnetic Properties of $(FexCo_{1-x})_{73.5}Cu1Mo_3Si_{13.5}B_9$ (X = 0.5, 1) Alloys. *J. Magn. Magn. Mater.* **2013**, *328*, 62–65. [CrossRef]
12. Mishra, D.; Perumal, A.; Saravanan, P.; Babu, D.A.; Srinivasan, A. Effect of Co or Mn Addition on the Soft Magnetic Properties of Amorphous Fe89− XZr11Bx (X = 5, 10) Alloy Ribbons. *J. Magn. Magn. Mater.* **2009**, *321*, 4097–4102. [CrossRef]
13. Torrens-Serra, J.; Bruna, P.; Roth, S.; Rodriguez-Viejo, J.; Clavaguera-Mora, M.T. Effect of Minor Co Additions on the Crystallization and Magnetic Properties of Fe (Co) NbBCu Alloys. *J. Alloy. Compd.* **2010**, *496*, 202–207. [CrossRef]
14. Müller, M.; Grahl, H.; Mattern, N.; Kühn, U.; Schnell, B. The Influence of Co on the Structure and Magnetic Properties of Nanocrystalline FeSiB–CuNb and FeZrBCu-Based Alloys. *J. Magn. Magn. Mater.* **1996**, *160*, 284–286. [CrossRef]

15. Inoue, A.; Shen, B.L.; Chang, C.T. Fe-and Co-Based Bulk Glassy Alloys with Ultrahigh Strength of over 4000 MPa. *Intermet. (Barking)* **2006**, *14*, 936–944. [CrossRef]
16. Komatsu, T.; Sato, S.; Matusita, K. Compositional Dependence of Resistivity Changes during Structural Relaxation in (Co, Fe) 75Si10B15 Metallic Glasses. *Acta Metall.* **1986**, *34*, 1899–1904. [CrossRef]
17. Hayashi, K.; Hayakawa, M.; Ochiai, Y.; Matsuda, H.; Ishikawa, W.; Iwasaki, Y.; Aso, K. Magnetic and Other Properties and Sputtering Behavior of Co-base Amorphous Alloy Films. *J. Appl. Phys.* **1987**, *61*, 2983–2992. [CrossRef]
18. Steeb, S. *Rapidly Quenched Metals*; Elsevier: Amsterdam, The Netherlands, 2012; Volume 1, ISBN 0444601112.
19. Chen, Y.M.; Ohkubo, T.; Ohta, M.; Yoshizawa, Y.; Hono, K. Three-Dimensional Atom Probe Study of Fe–B-Based Nanocrystalline Soft Magnetic Materials. *Acta Mater.* **2009**, *57*, 4463–4472. [CrossRef]
20. Inoue, A.; Shen, B. Soft Magnetic Bulk Glassy Fe-B-Si-Nb Alloys with High Saturation Magnetization above 1.5 T. *Mater. Trans.* **2002**, *43*, 766–769. [CrossRef]
21. Inoue, A.; Shen, B. Formation and Soft Magnetic Properties of Co-Fe-Si-B-Nb Bulk Glassy Alloys. *Mater. Trans.* **2002**, *43*, 1230–1234. [CrossRef]
22. Amiya, K.; Urata, A.; Nishiyama, N.; Inoue, A. Magnetic Properties of (Fe, Co)–B–Si–Nb Bulk Glassy Alloys with High Glass-Forming Ability. *J. Appl. Phys.* **2005**, *97*, 10F913. [CrossRef]
23. Urata, A.; Amiya, K.; Inoue, A. Glass-Forming Ability and Magnetic Properties of (Fe, Co)-B-Si-Nb Bulk Glassy Alloys. *J. Metastable Nanocrystalline Mater.* **2005**, *24*, 535–538. [CrossRef]
24. McHenry, M.E.; Willard, M.A.; Laughlin, D.E. Amorphous and Nanocrystalline Materials for Applications as Soft Magnets. *Prog. Mater. Sci* **1999**, *44*, 291–433. [CrossRef]
25. Kronmüller, H.; Fähnle, M.; Domann, M.; Grimm, H.; Grimm, R.; Gröger, B. Magnetic Properties of Amorphous Ferromagnetic Alloys. *J. Magn. Magn. Mater.* **1979**, *13*, 53–70. [CrossRef]
26. Luborsky, F.; Becker, J.; McCary, R. Magnetic Annealing of Amorphous Alloys. *IEEE Trans. Magn.* **1975**, *11*, 1644–1649. [CrossRef]
27. Kronmüller, H.; Fernengel, W. The Role of Internal Stresses in Amorphous Ferromagnetic Alloys. *Phys. Status Solidi (A)* **1981**, *64*, 593–602. [CrossRef]
28. Flohrer, S.; Schäfer, R.; Polak, C.; Herzer, G. Interplay of Uniform and Random Anisotropy in Nanocrystalline Soft Magnetic Alloys. *Acta Mater.* **2005**, *53*, 2937–2942. [CrossRef]
29. Makino, A.; Men, H.; Kubota, T.; Yubuta, K.; Inoue, A. FeSiBPCu Nanocrystalline Soft Magnetic Alloys with High Bs of 1.9 Tesla Produced by Crystallizing Hetero-Amorphous Phase. *Mater. Trans.* **2009**, *50*, 204–209. [CrossRef]
30. Roy, R.K.; Panda, A.K.; Mitra, A. Effect of Co Content on Structure and Magnetic Behaviors of High Induction Fe-Based Amorphous Alloys. *J. Magn. Magn. Mater.* **2016**, *418*, 236–241. [CrossRef]
31. Fornell, J.; González, S.; Rossinyol, E.; Suriñach, S.; Baró, M.D.; Louzguine-Luzgin, D.V.; Perepezko, J.H.; Sort, J.; Inoue, A. Enhanced Mechanical Properties Due to Structural Changes Induced by Devitrification in Fe–Co–B–Si–Nb Bulk Metallic Glass. *Acta Mater.* **2010**, *58*, 6256–6266. [CrossRef]
32. Gómez-Polo, C.; Marín, P.; Pascual, L.; Hernando, A.; Vázquez, M. Structural and Magnetic Properties of Nanocrystalline $Fe_{73.5-x}Co_xSi_{13.5}B_9CuNb_3$ Alloys. *Phys. Rev. B* **2001**, *65*, 024433. [CrossRef]
33. Kulik, T. The Influence of Copper, Niobium and Tantalum Additions on the Crystallization of Fe–Si–B–Based Glasses. *Mater. Sci. Eng. A* **1992**, *159*, 95–101. [CrossRef]
34. López, G.P.; Fabietti, L.M.; Condó, A.M.; Urreta, S.E. Microstructure and Soft Magnetic Properties of Finemet-Type Ribbons Obtained by Twin-Roller Melt-Spinning. *J. Magn. Magn. Mater.* **2010**, *322*, 3088–3093. [CrossRef]
35. Yoshizawa, Y.A.; Oguma, S.; Yamauchi, K. New Fe-based Soft Magnetic Alloys Composed of Ultrafine Grain Structure. *J. Appl. Phys.* **1988**, *64*, 6044–6046. [CrossRef]
36. Yoshizawa, Y.; Yamauchi, K. Magnetic Properties of Fe–Cu–M–Si–B (M = Cr, V, Mo, Nb, Ta, W) Alloys. *Mater. Sci. Eng. A* **1991**, *133*, 176–179. [CrossRef]
37. Fan, X.; Zhu, F.; Wang, Q.; Jiang, M.; Shen, B. Effect of Magnetic Field Annealing on Microstructure and Magnetic Properties of FeCuNbSiB Nanocrystalline Magnetic Core with High Inductance. *Appl. Microsc.* **2017**, *47*, 29–35. [CrossRef]
38. Mitra, A.; Panda, A.K.; Singh, S.R.; Rao, V.; Ramachandrarao, P. Magnetic and Structural Behaviours of Nanocrystalline $Fe_{70.8}Nb_{3.7}Cu_1Al_{2.7}Mn_{0.7}Si_{13.5}B_{7.6}$ Alloy. *Philos. Mag.* **2003**, *83*, 1495–1509. [CrossRef]
39. Herzer, G. Grain Structure and Magnetism of Nanocrystalline Ferromagnets. *IEEE Trans. Magn.* **1989**, *25*, 3327–3329. [CrossRef]
40. Yoshizawa, Y.; Fujii, S.; Ping, D.H.; Ohnuma, M.; Hono, K. Magnetic Properties of Nanocrystalline FeMCuNbSiB Alloys (M: Co, Ni). *Scr. Mater.* **2003**, *48*, 863–868. [CrossRef]
41. Inoue, A. Stabilization of Metallic Supercooled Liquid and Bulk Amorphous Alloys. *Acta Mater.* **2000**, *48*, 279–306. [CrossRef]
42. Inoue, A. High Strength Bulk Amorphous Alloys with Low Critical Cooling Rates (Overview). *Mater. Trans. JIM* **1995**, *36*, 866–875. [CrossRef]
43. Inoue, A. Bulk Amorphous Alloys with Soft and Hard Magnetic Properties. *Mater. Sci. Eng. A* **1997**, *226*, 357–363. [CrossRef]
44. Inoue, A.; Shen, B.L.; Chang, C.T. Super-High Strength of over 4000 MPa for Fe-Based Bulk Glassy Alloys in [(Fe1−XCox)0.75B0.2 Si0.05]96Nb4 System. *Acta Mater.* **2004**, *52*, 4093–4099. [CrossRef]
45. De Boer, F.R.; Boom, R.; Mattens, W.C.M.; Miedema, A.R.; Niessen, A.K. *Cohesion in metals, Transition Metal Alloys*; Noth-Holland: Amsterdam, The Netherlands, 1989.

46. Chang, C.; Shen, B.; Inoue, A. Co–Fe–B–Si–Nb Bulk Glassy Alloys with Superhigh Strength and Extremely Low Magnetostriction. *Appl. Phys. Lett.* **2006**, *88*, 011901. [CrossRef]
47. Kim, S.; Kim, Y.J.; Kim, Y.K.; Choi-Yim, H. Annealing Effect on the Magnetic Properties of Cobalt-Based Amorphous Alloys. *Curr. Appl. Phys.* **2017**, *17*, 548–551. [CrossRef]
48. Kwon, S.; Kim, S.; Choi-Yim, H.; Lee, D.; Kwon, S.; Kim, K. Effects of Fe Substitution for Co on the Thermal, Magnetic, and Mechanical Properties of the Co-Fe-B-Si-Mo Alloy System. *J. Korean Phys. Soc.* **2018**, *72*, 171–176. [CrossRef]
49. Schoen, M.A.W.; Lucassen, J.; Nembach, H.T.; Silva, T.J.; Koopmans, B.; Back, C.H.; Shaw, J.M. Magnetic Properties of Ultrathin 3 d Transition-Metal Binary Alloys. I. Spin and Orbital Moments, Anisotropy, and Confirmation of Slater-Pauling Behavior. *Phys. Rev. B* **2017**, *95*, 134410. [CrossRef]
50. Takahashi, C.; Ogura, M.; Akai, H. First-Principles Calculation of the Curie Temperature Slater–Pauling Curve. *J. Phys. Condens. Matter* **2007**, *19*, 365233. [CrossRef]
51. MacLaren, J.M.; Schulthess, T.C.; Butler, W.H.; Sutton, R.; McHenry, M. Electronic Structure, Exchange Interactions, and Curie Temperature of FeCo. *J. Appl. Phys.* **1999**, *85*, 4833–4835. [CrossRef]
52. Kwon, S.; Kim, S.; Yim, H. Improvement of Saturation Magnetic Flux Density in Fe–Si–B–Nb–Cu Nanocomposite Alloys by Magnetic Field Annealing. *Curr. Appl. Phys.* **2020**, *20*, 37–42. [CrossRef]
53. Chen, W.Z.; Ryder, P.L. X-Ray and Differential Scanning Calorimetry Study of the Crystallization of Amorphous Fe73. 5 Cu1Nb3 Si13. 5B9 Alloy. *Mater. Sci. Eng. B* **1995**, *34*, 204–209. [CrossRef]
54. Nabiałek, M. Soft Magnetic and Microstructural Investigation in Fe-Based Amorphous Alloy. *J. Alloy. Compd.* **2015**, *642*, 98–103. [CrossRef]
55. Marin, P.; Olofinjana, A.O.; Vázquez, M.; Davies, H.A. Influence of the As-Cast State on the Crystallization Process and Magnetic Properties for FeSiBCuNb Wires. *IEEE Trans. Magn.* **1994**, *30*, 4794–4796. [CrossRef]
56. Long, Z.; Shen, B.; Shao, Y.; Chang, C.; Zeng, Y.; Inoue, A. Corrosion Behaviour of $[(Fe_{0.6}Co_{0.4})_{0.75}B_{0.2}Si_{0.05}]$ 96Nb4 Bulk Glassy Alloy in Sulphuric Acid Solutions. *Mater. Trans.* **2006**, *47*, 2566–2570. [CrossRef]
57. Inoue, A.; Shen, B.L. A New Fe-based Bulk Glassy Alloy with Outstanding Mechanical Properties. *Adv. Mater.* **2004**, *16*, 2189–2192. [CrossRef]
58. Zhang, Y.; Zhao, X.; Bozzolo, N.; He, C.; Zuo, L.; Esling, C. Low Temperature Tempering of a Medium Carbon Steel in High Magnetic Field. *ISIJ Int.* **2005**, *45*, 913–917. [CrossRef]
59. Marin, P.; Vázquez, M.; Olofinjana, A.O.; Davies, H.A. Influence of Cu and Nb on Relaxation and Crystallization of Amorphous FeSiB (CuNb) Wires. *Nanostructured Mater.* **1998**, *10*, 299–310. [CrossRef]
60. Fan, C.; Yang, Y.; Xu, J.; Luo, T.; Wang, G. Effects of Nb Addition and Heat Treatment on the Crystallization Behavior, Thermal Stability and Soft Magnetic Properties of FeSiBPCuC Alloys. *J. Korean Phys. Soc.* **2020**, *77*, 116–121. [CrossRef]
61. Wang, A.D.; Men, H.; Shen, B.L.; Xie, G.Q.; Makino, A.; Inoue, A. Effect of P on Crystallization Behavior and Soft-Magnetic Properties of Fe83. 3Si4Cu0. 7B12− XPx Nanocrystalline Soft-Magnetic Alloys. *Thin Solid Film.* **2011**, *519*, 8283–8286. [CrossRef]
62. Herzer, G. Anisotropies in Soft Magnetic Nanocrystalline Alloys. *J. Magn. Magn. Mater.* **2005**, *294*, 99–106. [CrossRef]
63. Cremaschi, V.; Arcondo, B.; Sirkin, H.; Vazquez, M.; Asenjo, A.; Garcia, J.M.; Abrosimova, G.; Aronin, A. Huge Magnetic Hardening Ascribed to Metastable Crystallites during First Stages of Devitrification of Amorphous FeSiBNbSn Alloys. *J. Mater. Res.* **2000**, *15*, 1936–1942. [CrossRef]
64. Luborsky, F.E. Amorphous Metallic Alloys. *Amorph. Met. Alloy.* **1983**, *1*.

Disclaimer/Publisher's Note: The statements, opinions and data contained in all publications are solely those of the individual author(s) and contributor(s) and not of MDPI and/or the editor(s). MDPI and/or the editor(s) disclaim responsibility for any injury to people or property resulting from any ideas, methods, instructions or products referred to in the content.